The International Journal of Advanced Manufacturing Technology
https://doi.org/10.1007/s00170-020-04945-3

ORIGINAL ARTICLE

On the impacts of tool geometry and cutting conditions in straight turning of aluminum alloys 6061-T6: an experimentally validated numerical study

Mahshad Javidikia [1] · Morteza Sadeghifar [2] · Victor Songmene [1] · Mohammad Jahazi [1]

Received: 15 October 2019 / Accepted: 15 January 2020

Authors' accepted manuscript
Article published in *The International Journal of Advanced Manufacturing Technology* 2020, volume 106, pages 4547–4565
https://doi.org/10.1007/s00170-020-04945-3

On the Impacts of Tool Geometry and Cutting Conditions in Straight Turning of Aluminum Alloys 6061-T6: An Experimentally Validated Numerical Study

Mahshad Javidikia[a], Morteza Sadeghifar[b], Victor Songmene[a, *], Mohammad Jahazi[a]

[a]*Department of Mechanical Engineering, École de Technologie Supérieure, Montreal, Canada*
[b]*Department of Mechanical, Industrial and Aerospace Engineering, Concordia University, Montreal, Canada*
* Corresponding author. *E-mail address: victor.songmene@etsmtl.ca*

Abstract

Aluminum alloys 6061-T6 are widely utilized in the automotive, aerospace and marine industries due to high corrosion resistance, high strength, and good workability and machinability. The machining performance of these alloys depend on several factors including tool's material, coating and geometry. Cutting tool edge radius is one of the most effective factors in cutting forces, energy requirement and chip formation during metal cutting. The present article aims to study the interactions between the cutting edge radius and cutting speed, feed rate and rake angle and examine the impacts of the aforementioned tool geometry and cutting conditions on machining forces, cutting temperature, and chip thickness in cutting an aluminum alloy 6061-T6. Special attention is devoted to examining the influence of the cutting edge radius on machining variables and comparing the results of conventional machining (CM) and high speed machining (HSM). A finite element model was developed to simulate the above intercations and was experimentally validated for different machining parameters. The results demonstrate that although increasing the cutting edge radius clearly raises the machining forces, it has a slight influence on the chip thickness. It is also found that the maximum cutting temperatures remain nearly constant with changes in the tool edge radius, while the average temperatures of the tool tip increase especially in HSM. Furthermore, it was found that the location at which the maximum cutting temperature occurs depends more on cutting conditions and tool geometry than workpiece and tool materials.

Keywords: *Aluminum alloy 6061-T6. Straight Turning. Tool Edge Radius. Finite Element Method*

1. Introduction

Machining of metals is often accompanied by non-uniform cutting temperatures and machining forces, producing residual stresses. These temperatures and forces may lead to inaccuracies in component

dimensions, raise the power consumption of machine tools, cause tool wear and damage, result in an excessive deflection and breakage of the tool.

In orthogonal machining, various factors including cutting conditions (cutting speed and feed rate) and tool geometry (rake angle and edge radius) can affect machining characteristics and surface quality. In recent years, with the advent of HSM equipment, the aerospace industry is adopting HSM due to its merits over CM processes. However, in order to minimize the trial and error approach and mitigate the investment risks, it is of high importance to quantify the impact of various HSM processing on critical machining variables. Using FE models enables manufacturers to address the above concerns and predict the influence of machining conditions on characteristics such as cutting forces, temperature and chip morphology.

Yen et al. [1] performed a finite element analysis based on an updated Lagrangian formulation using the DEFORM® software to examine the effect of tool edge geometry on machining characteristics in orthogonal machining of AISI 1020 steels. They found that increasing cutting edge radius slightly increased the chip thickness, whereas it had almost no effect on the magnitude of the maximum tool temperatures near the tool tip. Özel [2] carried out FE simulations of orthogonal turning of Inconel 718 based on the modified Johnson-Cook material model using the DEFORM® software. They found that a larger tool edge radius produced higher specific cutting forces and temperatures and a smaller edge radius with neutral rake angle resulted in lower forces and temperatures.

Wyen and Wegener [3] experimentally studied the influence of cutting edge radius on cutting forces in machining titanium alloys and reported that the cutting and feed forces increased with raising cutting edge radius. Daoud et al. [4] conducted research on the influence of the rake angle on cutting process parameters of Al2024-T3 alloy induced by orthogonal machining using the DEFORM® software. They reported that the cutting forces decreased by 55% with changing the rake angle from −8° to +8°.

Cheng et al. [5] conducted a numerical study of orthogonal cutting Fe-Cr-Ni stainless steel using the AdvantEdge™ software to analyze the machining charactrestics in the workpiece and tool for different cutting edge and rake angle values. The results showed that the cutting edge radius had little and great effects on the temperature and stress, respectively. In addition, the highest temperature in the tool gradually increased and the tool stress first decreased and then increased with the increase of the rake angle. Akram et al. [6] numerically and experimentally investigated the effect of cutting speed and feed rate on the chip thickness of aluminum alloys 6061 produced by orthogonal machining operations. They concluded that the chip thickness diminished and increased with increasing cutting speed and feed rate, respectively.

Zhuang et al. [7] developed a finite element model to study the influences of the chamfer length, chamfer angle and feed rate (uncut chip thickness) on the cutting forces in orthogonal cutting of Ti6Al4V and Inconel 718 using the AdvantEdge™ software. A new calibration model for the edge coefficients was used to consider the effect of the chamfered edge and length to predict the edge force components. The results demonstrated that the chamfered length and angle had a considerable effect on the cutting forces. Reddy et al. [8] conducted the FE simulation of the orthogonal turning of Ti6Al4V alloy using the AdvantEdge™ software. The results showed that the tool edge radius had a considerable effect on cutting forces and temperature. They also reported that when the cutting tool edge radius decreased, high thermal stress was observed on the cutting tool.

Emamian [9] developed a FE model of orthogonal turning of AISI 1045 steel based on an updated Lagrangian approach using the Abaqus®/Explicit software. They found that the machining forces increased with the feed rate for various edge radii. Moreover, increasing the cutting edge radius led to a larger maximum cutting temperature except for the lowest feed rate. Patel [10] carried out a numerical research on FE modeling of orthogonal turning of aluminum alloy AA2024-T351 using the Abaqus® software. The Johnson-Cook damage model and the Hillerborg's fracture model were used to consider damage initiation and damage evolution in the workpiece material, respectively. The results displayed that the average cutting force increased with increasing the feed rate (uncut chip thickness) and decreasing the tool rake angle. Moreover, the average cutting force decreased slightly with increase in the cutting speed. The cutting temperature in primary and secondary shear zones diminished when the tool rake angle was increased. It needs mentioning that the effect of tool cutting edge radius was not investigated in this study and the model was validated using the data available in the open literature.

Mir et al. [11] performed the FE simulations in single point diamond turning of silicon based on the smoothed particle hydrodynamics approach and the Drucker-Prager material constitutive model using the Abaqus® software. The results indicated that the cutting force ratio first increased and then decreased for the rake angles from -25^{o} to -30^{o} and from -35^{o} to -40^{o}, respectively. Jiang and Wang [12] carried out the finite element simulation to examine the performance of various wiper tool edge geometries in orthogonal machining of AISI 4340 steel. The cutting process was simulated based on Arbitrary-Lagrangian-Eulerian approach using the AdvantEdge™ software. The results demonstrated that the wiper tool reduced the temperature of the tool's flank face compared with the hone conventional tool, while it increased the temperature of the rake face and the cutting force.

The above overview of the previous studies shows that the impact of cutting edge radius on machining characteristics depend highly on work materials, cutting conditions, and tool geometry. Furthermore, little data is available on the interaction between the edge radius and cutting speed, rake angle and feed

rate and their influences on machining characteristics, especially in the range of high speed machining of aluminum alloys [13].

The main objective of the present research study is to assess the interaction between the cutting edge radius and cutting speed, rake angle and feed rate and their impacts on machining charactrestics in orthogonal high speed turning of aluminum alloy 6061-T6. Particularly, the influence of the cutting edge radius on the location and magnitude of maximum cutting temperature and chip thickness in high speed machining of aluminum alloy 6061-T6 will be studied. The influence of tool edge radius on machining performance between conventional machining and high speed machining will also be investigated in the present work to better illustarte the differences between the two techniques. To achieve these, the cutting speeds of 361, 650, 950 and 1250 m/min, the feed rates of 0.1, 0.16 and 0.2 mm/rev, the rake angles of -8^o, 0^o and +8^o, and the cutting edge radii of 0.005, 0.01, 0.02, 0.03 and 0.04 mm will be considered. The first two cutting speeds lead to CM and the second two ones result in HSM.

2. Experimental tests

Dry orthogonal straight turning tests were carried out on a MAZAK CNC machine. The workpiece was a 150-mm diameter and 120-mm length cylinder made of aluminum alloy 6061-T6 and the tool was uncoated carbide (ISO CCGX 120408-AL H10). A right-hand tool holder of SCLCR 2020 K12 was employed to hold the inserts, as shown in Fig. 1a. A new insert was used for each machining experiment to provide similar conditions for all the tests. The workpiece components were groove machined to form tube-shaped samples with a 4-mm thickness. The machining tests were carried out for the cutting conditions listed in Table 1 with the tool geometry including the edge radius of r_β=0.02 mm, the rake angle of γ_0= 17.5 degrees, and the clearance angle of α_0 = 7 degrees. Machining forces were measured using a Kistler (type 9121) three-component piezoelectric dynamometer. The acquisition of force signals was conducted with a LabVIEW software and data treatment was performed using MATLAB codes. The chip thickness was measured using a digital micrometer by averaging the values of the chip thickness at three different locations far enough from the two ends of the chip. A HITACHI TM3000 Scanning Electron Microscope (SEM) was utilized to observe the chip shape. The experimental set-up of the orthogonal straight turning tests is displayed in Fig. 1b.

3. Finite element modeling

In the present study, Finite Element Method (FEM) was utilized to simulate the orthogonal straight turning of aluminum alloys 6061-T6 using the DEFORM software. The mathematical formulation of the analysis is based on an updated Lagrangian formulation and implicit integration method for large plastic

deformation analysis. In the present section, these formulations together with the characteristics of the developed FE model are described.

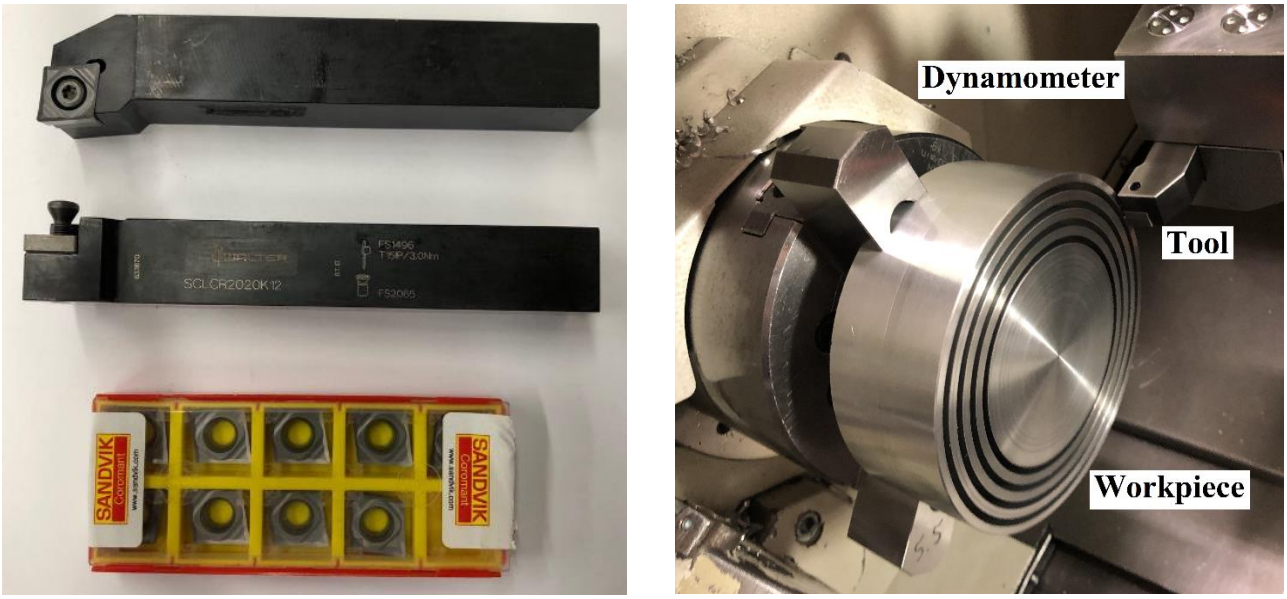

(a) (b)

Fig. 1. (a) The insert and toolholder and (b) the experimental set-up of orthogonal machining.

Table 1 Cutting conditions for tool geometry including r_β=0.02 mm, γ_0=17.5°, and α_0=7°

Test No.	$V(m/\text{min})$	$f(mm/rev)$
1	361	0.16
2	650	0.16
3	950	0.16
4	1250	0.16
5	950	0.1
6	950	0.2

The equations of motion during cutting may be expressed at a specific instant of time as [14]:

$$[M]\{\ddot{U}\} + \{R_{\text{int}}\} = \{R_{ext}\} \quad (1)$$

where $[M]$ is the mass matrix, $\{\ddot{U}\}$ is the acceleration vector ($\{U\}$ is the displacement), and $\{R_{\text{int}}\}$ and $\{R_{ext}\}$ are the vectors of internal and external forces, respectively. The effect of damping is ignored, and consequently, $\{R_{\text{int}}\}$ is equal to

$$\{R_{\text{int}}\} = [C_d]\{\dot{U}\} + [K_s]\{U\} \cong [K_s]\{U\} \text{ where } [C_d] \cong 0 \quad (2)$$

where $[C_d]$ and $[K_s]$ are the damping and stiffness matrices, respectively. In addition, $\{R_{ext}\}$ involves the external forces applied during cutting including the reaction forces at the supports.

Heat transfer occurring during the machining process is described as [14]:

$$[C_T]\{\dot{T}\} + [K_T]\{T\} = \{\dot{Q}_g\} \tag{3}$$

in which $[C_T]$ and $[K_T]$ are the volumetric heat capacitance and thermal conduction matrices, respectively. Also, $\{\dot{Q}_g\}$ is the total heat generation in the machining process.

The thermal contact between the tool and workpiece is defined using the heat conduction through the tool-chip contact face from the chip to the tool during the cutting process which is calculated as:

$$Q = h_{\text{int}}\,(T_{wp} - T_t) \tag{4}$$

where h_{int} is heat transfer coefficient, T_{wp} and T_t are the workpiece and tool's temperature at the tool-chip interface. In the current research, a heat transfer coefficient of 10^7 $W/m^2\,{}^oC$ was calibrated for modeling and an initial temperature of 20 °C (room temperature) was applied to both tool and workpiece.

The convection heat transfer takes place between the workpiece surface and the ambient according to the following formulae [14]:

$$Q = h\ (T_{wp} - T_a) \tag{5}$$

in which h is convection heat transfer coefficient, and T_{wp} and T_a are the workpiece and ambient (room) temperature. In the present work, h was chosen as 20 $W/m^2\,{}^oC$.

It is known that the material models used in finite element modeling of machining processes cannot be identified using quasi-static tests. This is because the workpiece material undergoes high strain, strain rate, and temperature during machining. Several material constitutive models were commonly used in FE simulations of cutting such as Johnson-Cook, Zerilli-Armstrong, and Marusich models. The Johnson-Cook material constitutive model has been extensively used in machining simulations and it was proved to be appropriate in modelling the machining processes [15,16].

In addition, the Johnson-Cook constitutive equation was used for modeling plastic deformation of the workpiece material as follows:

$$\bar{\sigma} = [A + B(\varepsilon)^n]\left[1 + C\ln\left(\frac{\dot{\varepsilon}}{\dot{\varepsilon}_0}\right)\right]\left[1 - \left(\frac{T - T_{room}}{T_{melt} - T_{room}}\right)^m\right] \tag{6}$$

where ε is the plastic strain, $\dot{\varepsilon}$ the plastic strain rate (s^{-1}), $\dot{\varepsilon}_0$ the reference plastic strain rate (s^{-1}), $T({}^oC)$ the workpiece temperature, $T_{melt}({}^oC)$ the melting temperature of the workpiece, and $T_{room}({}^oC)$ the room temperature. Also, A (MPa) is the initial yield strength, B (MPa) the hardening

modulus, C the strain rate sensitivity coefficient, n the hardening coefficient, and m the thermal softening coefficient. Table 2 lists the Johnson-Cook constants of aluminum alloy 6061-T6.

Table 2 The constants of Johnson-Cook material model of aluminum alloy 6061-T6 [17]

$A\ (MPa)$	$B\ (MPa)$	n	C	m	$\dot{\varepsilon}_0\ (1/s)$	$T_{melt}\ (^oC)$	$T_{room}\ (^oC)$
250	79.70	0.499	0.0249	1.499	1	652	20

Modeling of frictional behavior at the tool-workpiece contact areas is a great challenge in finite element simulations of metal cutting processes. Three main frictional models commonly used in FE modeling of machining processes are presented in Table 3. The Coulomb friction model represents the relation between frictional stress τ and normal stress σ_n. The constant shear friction model assumes that the frictional stress on the rake face of the tool is proportional to the shear yield stress of the workpiece. The Zorev model estimates the friction at the tool-chip interface using constant shear friction model in sticking region and constant Coulomb friction model in sliding region.

Previos research shows that aluminum alloys are prone to adhering to the tool at the tool-chip interface during cutting [18], which indicates a sticking zone. The Coulomb and Zorev models are not capable of predicting precisely since there is no relative sliding at the tool-chip interface. As s rersult, the shear friction model with a constant coefficient between 0.8 and 0.9 was utilized in the present research study. Based on the difficulty and inaccuracy of friction coefficient measurements, this coefficient was often determined by calibrating the FE model based on comparing and matching the FE results with the corresponding experimental ones.

Table 3 Friction models frequently employed in FE simulations of machining processes [13]

Model	Formulae[1]
Coulomb friction model: Constant Coulomb friction coefficient at the entire tool-chip interface	$\tau = \mu\sigma_n$
Shear friction model: Constant shear friction coefficient at the entire tool-chip interface	$\tau = m\tau_Y$
Zorev model: Constant shear friction coefficient in sticking region and constant Coulomb friction coefficient in sliding region	$\tau = \tau_Y$ when $\mu\sigma_n \geq \tau_Y$, $0 < x \leq l_p$ $\tau = \mu\sigma_n$ when $\mu\sigma_n < \tau_Y$, $l_p < x \leq l_c$

[1] τ is shear stress, m shear friction factor, μ Coulomb friction coefficient, σ_n normal compressive stress, τ_Y shear flow stress, l_p and $l_c - l_p$ are the lengths of the sticking and sliding regions

For the simulation purposes, a 4.75 mm × 1.12 mm rectangle workpiece with an elastic-plastic behavior was considered. The workpiece was meshed with 6000 linear quadrilateral elements. The tool material was considered as a rigid body and was meshed with 1700 elements. Figure 2 illustrates the tool and workpiece's geometries. The workpiece and tool's material properties are given in Table 4. Figure 3 shows the boundary conditions (BCs) defined for the workpiece and the tool. In both horizontal and

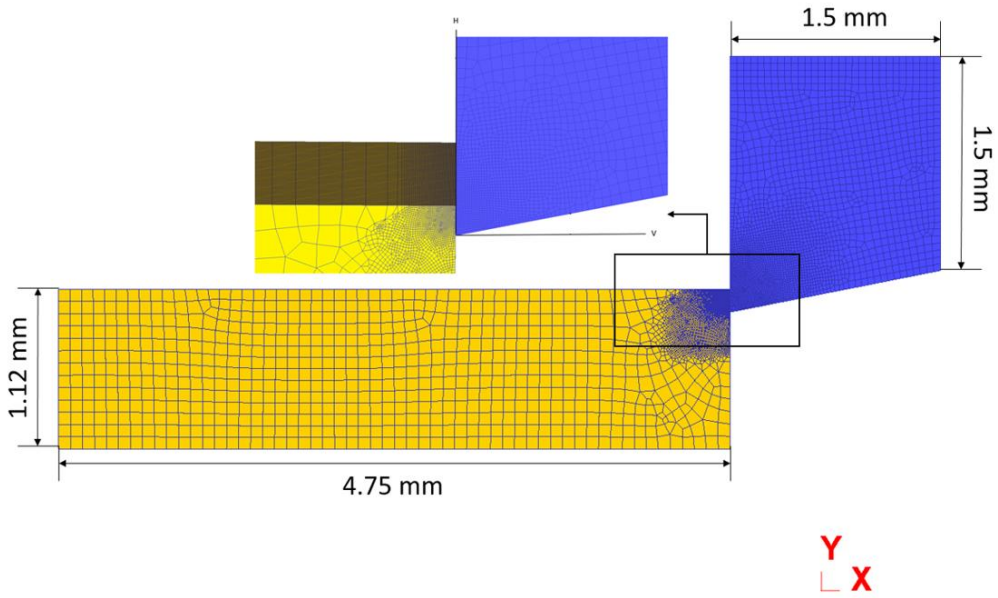

Fig. 2. The geometry and dimensions of the tool and workpiece in FE modeling.

Table 4 Mechanical and thermal properties of the workpiece and tool [19]

Properties	AA6061-T6	Uncoated carbide
Density $\rho\ (kg/m^3)$	2700	11900
Young's modulus $E\ (GPa)$	58.5	612
Poisson's ratio υ	0.33	0.22
Conductivity $k\ (W/m\ ^oC)$	167	86
Specific heat capacity $c\ (J/kg\ ^oC)$	896	337
Thermal expansion coefficient $\alpha\ (1/\ ^oC)$	23.5×10^{-6}	4.9×10^{-6}

vertical directions, the top and right sides of the cutting tool are fixed ($V_x = 0$ and $V_y = 0$, respectively). In addition, the bottom and left sides of the workpiece are fixed just in vertical direction ($V_y = 0$). The workpiece material moves through the fixed tool in the horizontal direction with a determined feed rate. The sides of the workpiece and tool which are far from the cutting zone and are retained at ambient temperature (T_{room}) of 20°C. Finally, continuous chip formation was assumed for all the simulations.

This assumption can be justified based on the experimental observations of chips for all the selected cutting conditions. The simulations were performed using a computer system of Intel® Xeon® CPU E3-1225 V5 with a CPU speed of 3.30 GHz and a memory RAM of 64.0 GB.

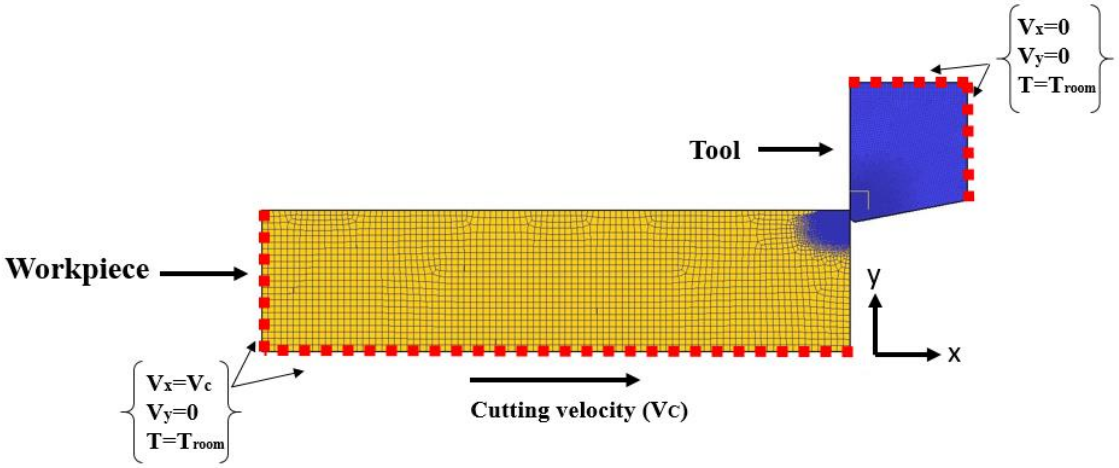

Fig. 3. The thermal and mechanical boundary conditions of the workpiece and tool.

4. Validation of the FE model

The developed finite element model is validated by comparing the present numerical results of chip thickness (t_c), cutting force (F_c), and thrust force (F_t) with those obtained through above-mentioned experimental tests. The predicted and experimental chip thicknesses are compared in Fig. 4a and good agreement is observed. Also, as shown in Fig. 4b, the simulated and measured cutting and thrust forces are well matched. For instance, for Test No. 5, Fig. 5 shows the distribution of cutting temperature in the workpiece and tool, where the steady-state condition is realized. Also, the experimental and simulated chip shapes for this test are both continuous as displayed in Figs. 6a and b. In addition, the machining forces for Test No. 5 are compared in Figs. 7a, b and c. As observed, there exists good agreement between the experimental and FE results. This was achieved by exploring diffrenet values of the shear friction coefficient and the heat transfer coefficient, and selecting aproprate coefficients using calibration of the FE results with the experimental ones. Moreover, mesh windows were assigned to the workpiece and the tool in order to have a high-quality fine mesh in the machined workpiece's surface and near-surface.

The validity of the developed FE model is additionally verified using the orthogonal cutting tests by Monzer et al. [17], whose machining conditions are given in Table 5. In [17], the same workpiece and tool's materials as those of the present study were utilized while different tool geometry parameters were used. As shown in Figs. 8a and b, the present FE results are in good agreement with the experimental ones presented in [17]. Previous research studies [1,20] showed that the discrepancy between the

simulated and measured thrust forces is unavoidable due to a lack of accurate friction and material constitutive models.

It should be emphasized that the developed FE model is validated with the present experiments for different cutting conditions including cutting speeds and feed rates and fixed tool geometry parameters (Figs. 4a and b). To verify the correctness of the FE model for different tool geometry parameters, the predicted machining forces and chip thicknesses are compared with the previous experimental ones for additional tool geometry parameters including tool edge radius, rake angle, and clearance angle (Figs. 8a and b).

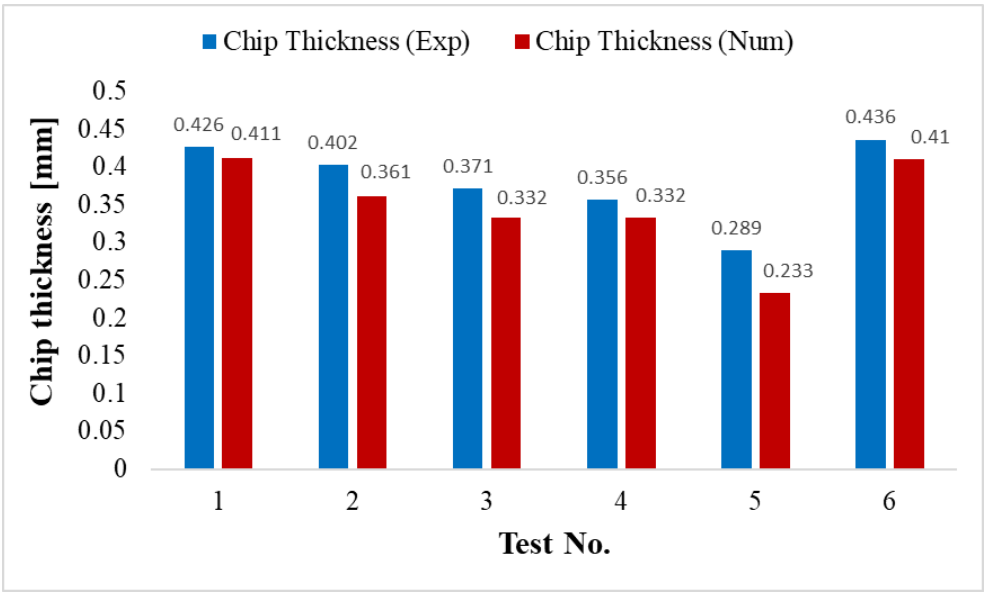

(a)

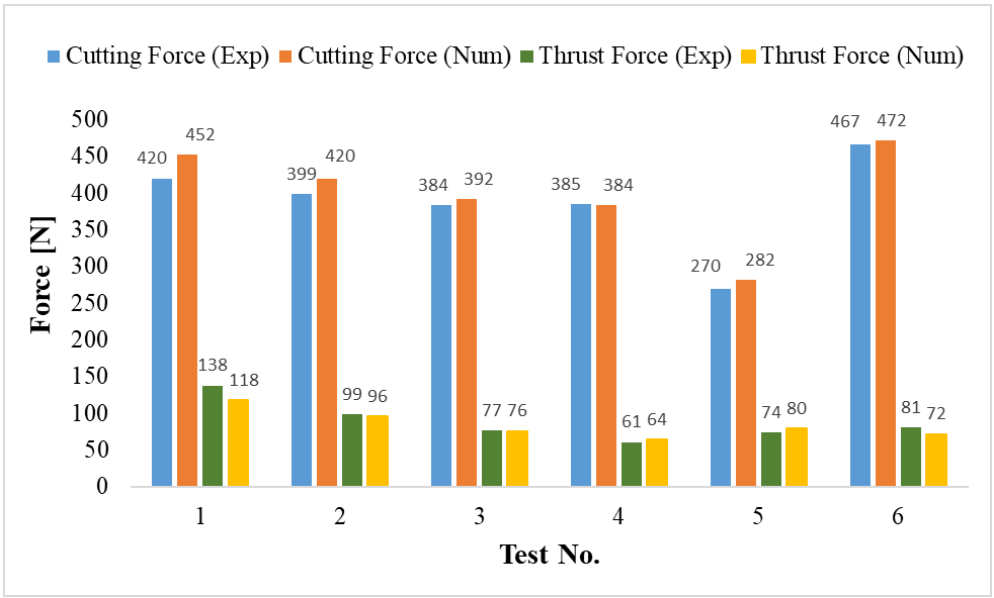

(b)

Fig. 4. Validation of the FE results of (a) chip thickness and (b) machining forces with the experimental ones.

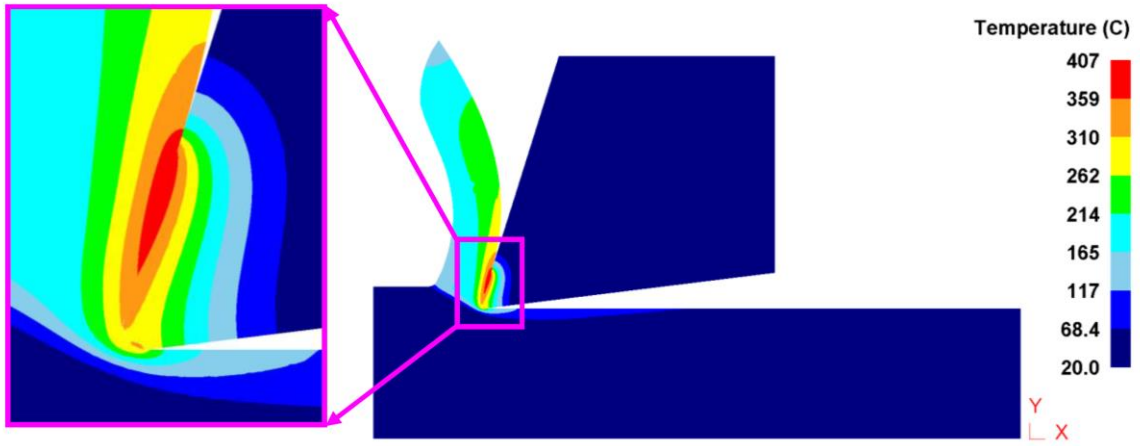

Fig. 5. The distribution of cutting temperature in the workpiece and tool for steady-state condition.

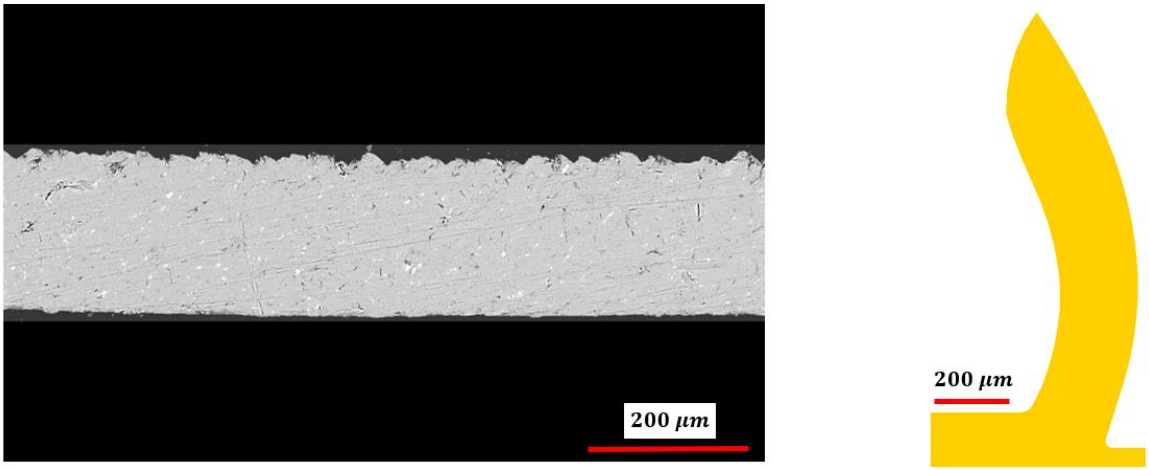

(a) (b)

Fig. 6. A comparison of (a) experimentally observed and (b) numerically simulated chip shapes.

Table 5 Cutting conditions and tool geometry [17]

Test No.	Cutting speed $V(m/\text{min})$	Feed rate $f(mm/rev)$	Edge radius $r_\beta(mm)$	Rake angle $\gamma_0(\text{deg})$	Clearance angle $\alpha_0(\text{deg})$
1	361	0.16	0.005	0	11
2	650	0.16	0.005	0	11
3	950	0.16	0.005	0	11
4	1250	0.16	0.005	0	11
5	950	0.16	0.005	-8	11
6	950	0.16	0.005	+8	11
7	950	0.1	0.005	0	11
8	950	0.2	0.005	0	11

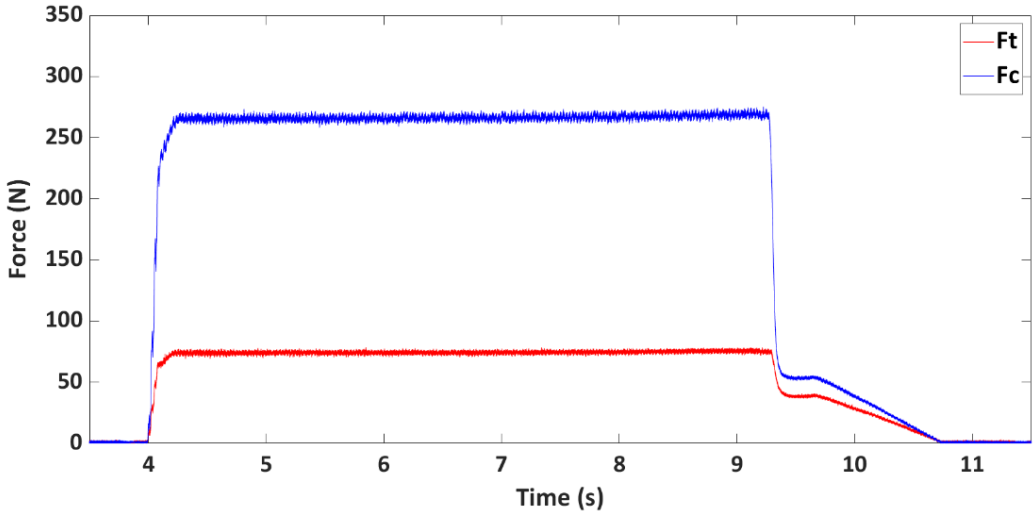

(a)

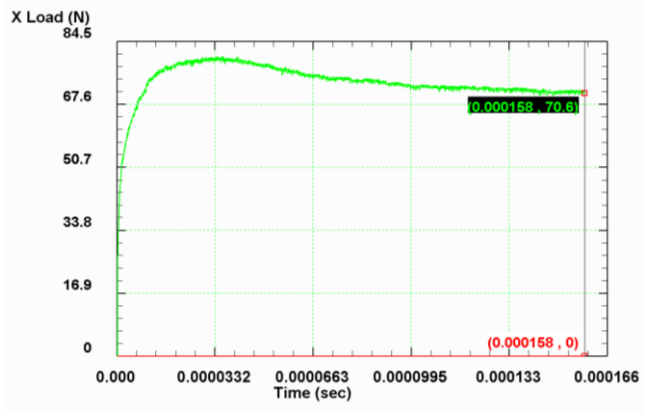

(b) Fc

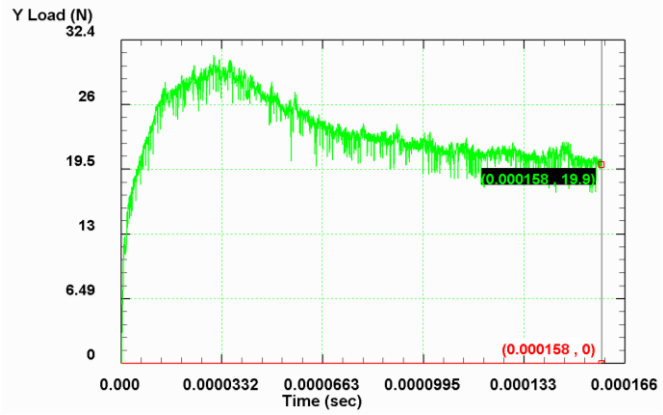

(c) Ft

Fig. 7. Variation of cutting and thrust forces with time during the cutting process:
(a) In the experiment (force signals) for the 4-mm width of cut and (b,c) in FE modeling for the unit width of cut.

5. Results and discussion

5.1. Interaction between cutting speed and cutting edge radius

Figure 9 illustrates the tool's cutting edge and different edge radii utilized in this research. Machining forces decrease or remain almost constant with increasing the cutting speed, as seen in Figs. 10 and 11. Specifically, there is a large reduction in both cutting and feed forces from the cutting speed of 361 m/min to other higher speeds. This can be attributed to the resultant of two facts. The first fact is that a higher cutting speed generates larger frictional and plastic works, yielding more thermal softening, and as a result, produces smaller cutting forces during machining [14,21]. In contrast, the second fact is that a high cutting speed causes a greater material removal rate, leading to a lower cutting temperature and larger cutting forces [14,22]. In a cutting process, the contribution of the first above-mentioned fact is greater than or almost equal to that of the second one, depending on the range in which the magnitude of

the cutting speed changes [14]. Specifically, as observed in Figs. 10 and 11, the effect of the cutting speed on the machining forces is smaller at higher cutting speeds of 950 and 1250 m/min, demonstrating that machining forces are more dependent on the cutting speed in CM than in HSM.

Machining forces increase with raising the cutting edge radius for all the four cutting speeds considered. The variations of the cutting and feed forces with the edge radius are linearly approximated

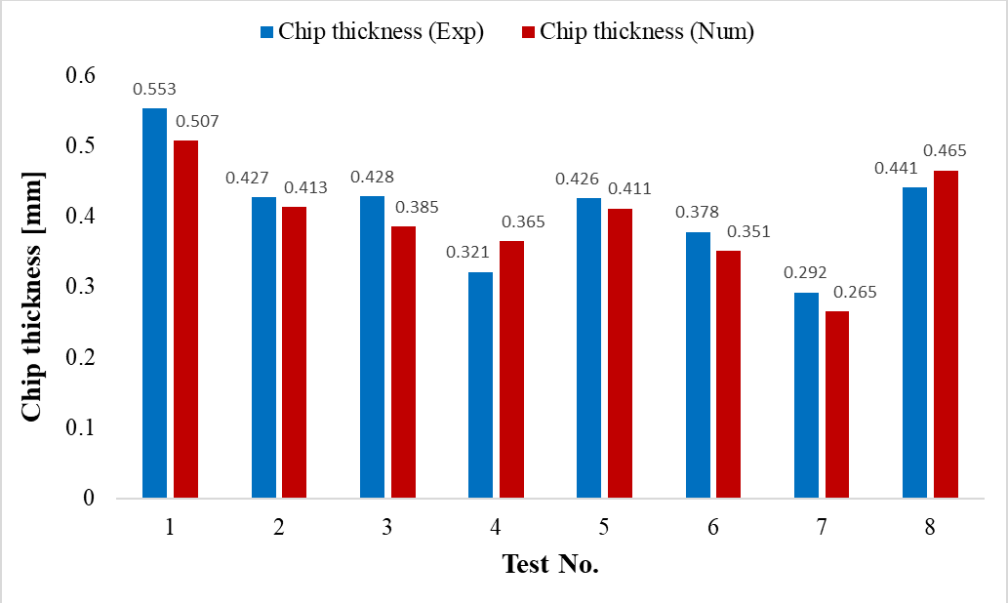

(a)

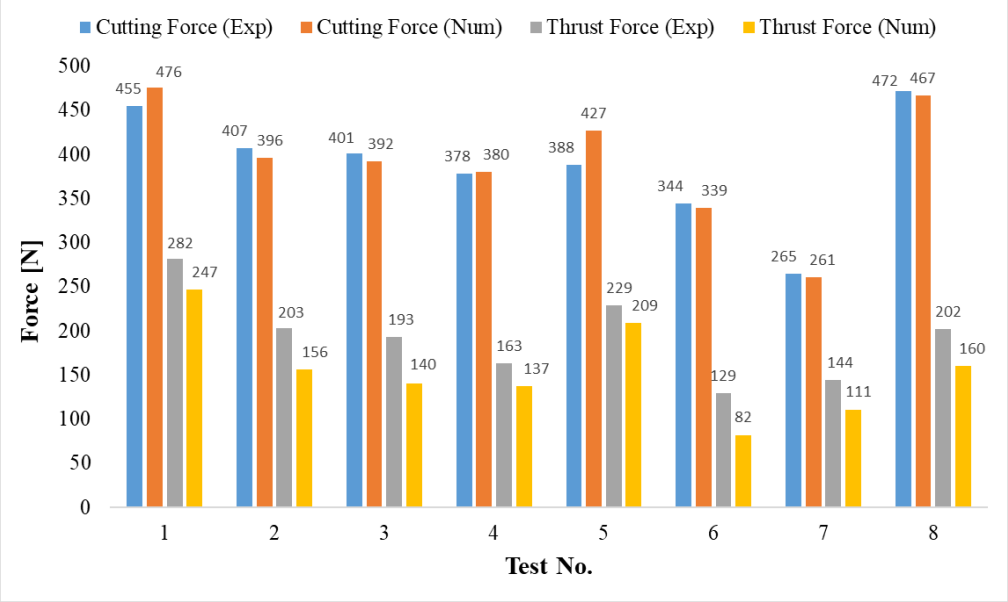

(b)

Fig. 8. Verification of the validity of the present FE results of (a) chip thickness and (b) machining forces with the previously published experimental ones [17].

as displayed in Figs. 10 and 11. Fitting linear regression models to the results assists to compare the variation's trends in responses more easily and efficiently. As observed in Figs. 10 and 11, the slope of the linear model at the cutting speed of 361 m/min is much higher for both cutting and feed forces (the slope is 1880 and 2842 for cutting and feed forces, respectively). This shows that both cutting and feed forces are more sensitive to the cutting edge radius at low cutting speeds which fall into CM. On the other hand, the slopes of the linear models of variations of the feed forces are larger than those of variations of the cutting forces. This reveals that the increase in the feed force is much larger than that in the cutting force for all the cutting speeds when the cutting edge radius is increased.

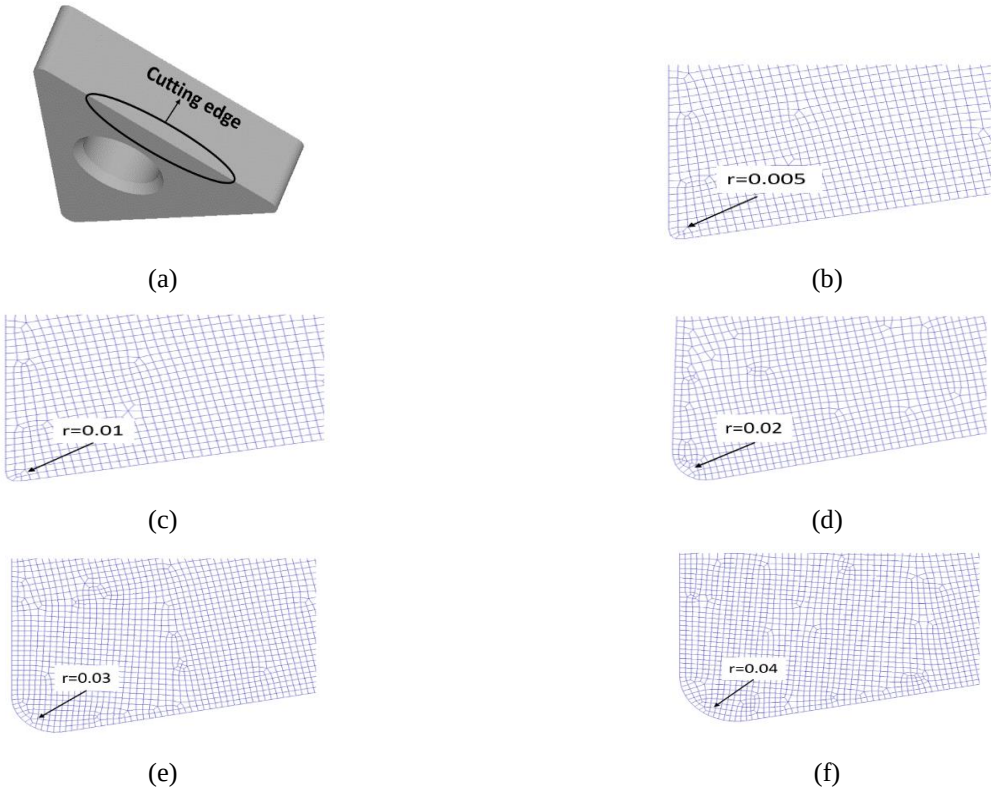

Fig. 9. The tool's cutting edge and different edge radii (in terms of mm).

The influences of cutting speed and cutting edge radius on cutting temperature are displayed in Figs. 12 and 13, where it can be seen that both the maximum temperature which occurs at the tool rake face (as shown in Fig. 5) and the average temperature of the tool tip rise with the cutting speed. This is due to the fact that a larger cutting speed generates higher frictional and plastic works, leading to higher temperatures, as mentioned previously.

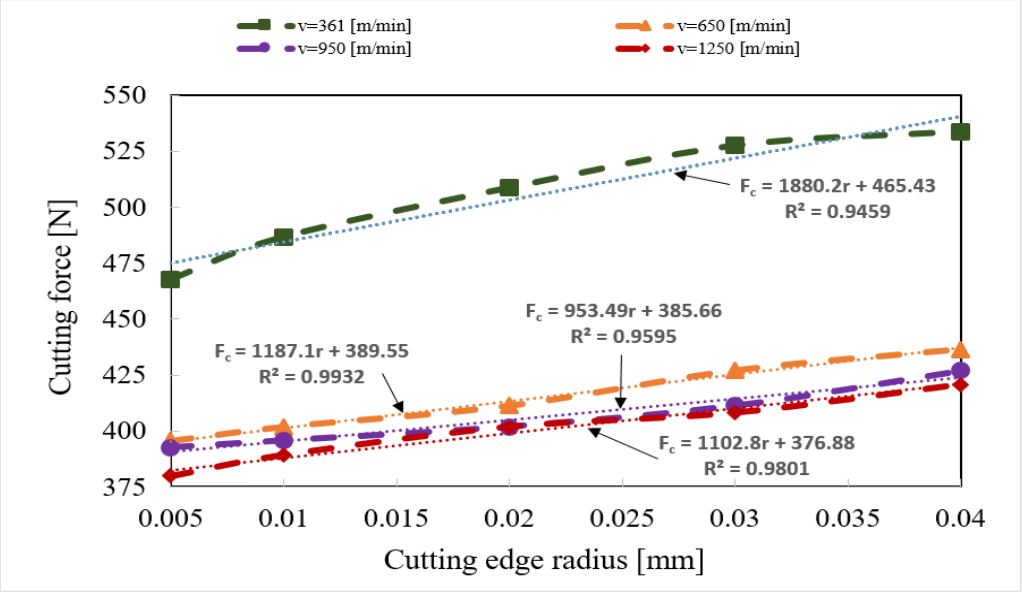

Fig. 10. The effect of cutting edge radius and cutting speed on cutting force.

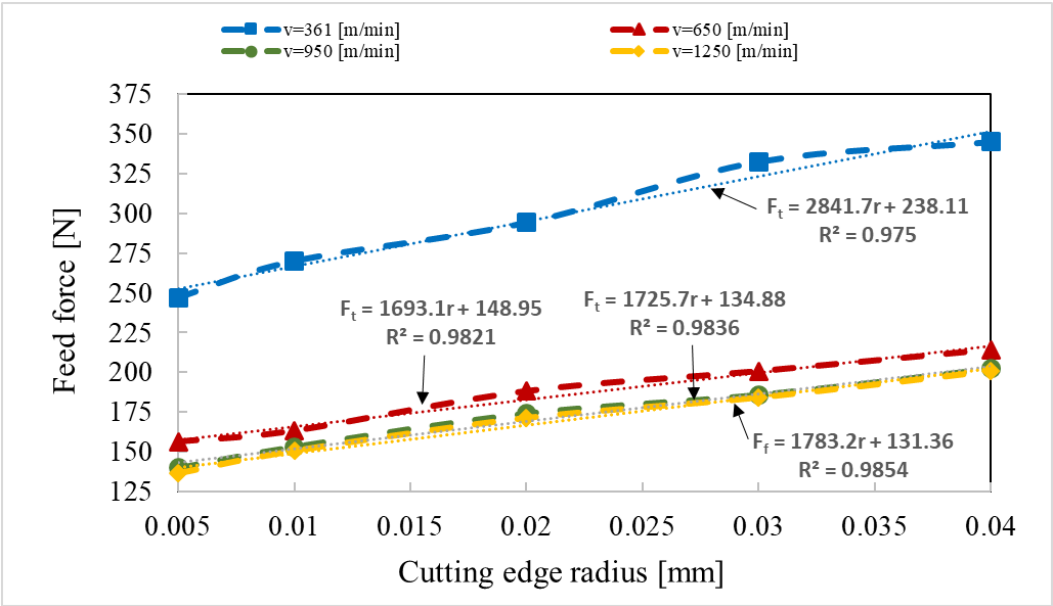

Fig. 11. The effect of cutting edge radius and cutting speed on feed force.

On the other hand, at low cutting speeds (361 and 650 m/min) which fall into CM, there are almost no differences between the magnitudes of the average temperature of the tool tip. By contrast, at high cutting speeds (950 and 1250 m/min) corresponding to HSM conditions, there are larger differences between the values of the average temperature of the tool tip. This shows that the influence of the cutting speed on the average temperature of the tool tip increases with raising the cutting speed. It must be mentioned that linear regression models for the maximum cutting temperatures are not provided here as

these temperatures reamin nearly constant with increasing the tool edge radius for all the cutting speeds under study, as seen in Fig. 12. In contrast, as viewed in Fig. 13, the average temperatures of the tool tip increase with the edge radius. This is better illustrated at the high speeds of 950 and 1250 m/min, in which the slopes of the linear models are higher than those related to the cutting speeds of 361 and 650 m/min. It is interesting to note that these results can be compared with those reported by Yen et al. [1], Özel and Zeren [23], and Al-Zkeri et al. [24], who examined the impact of the tool edge radius on cutting temperature.

The orthogonal cutting of AISI 1020 steel with uncoated carbide, AISI 4340 steel with uncoated carbide, and AISI 4142H steel with TiAlN-coated carbide was analyzed by Refs. [1], [23] and [24], respectively. According to the results of Ref. [1], the maximum temperature in cutting of AISI 1020 steel took place at the tool tip, as shown in Fig. 14a, contrary to the present results for aluminum alloys AA6061-T6. In contrast, based on the results reported in Refs. [23] and [24], as displayed in Fig. 14b and c, the maximum temperature in cutting of AISI 4340 steel and AISI 4142H steel occurred on the tool rake face, which is in agreement with the present results for aluminum alloys AA6061-T6. Also, the temperature of the tool tip in machining of AISI 1020 steel was not sensitive to the size of the edge radius [1], while the temperature of the tool rake face increased with raising the edge radius, opposite to the present results for aluminum alloys AA6061-T6. On the other hand, the tool rake face's temperature was not sensitive to the size of the edge radius in machining AISI 4340 steel [23], being in excellent agreement with the results for aluminum alloy AA6061-T6. In machining AISI 4142H steel, the temperature of the tool rake face slightly rose with raising the edge radius. These comparisons demonstrate that the location of the maximum cutting temperature and the sensitivity of the maximum cutting temperature to the cutting edge radius in metal cutting depend more on cutting conditions and tool geometry than workpiece and tool materials.

The effects of cutting speed and cutting edge radius on chip thickness were also investigated. As shown in Fig. 15, the chip thickness decreases when the cutting speed increases. This is because increasing the cutting speed increases the shear angle, and consequently, diminishes the chip thickness. Similar to the behaviors of the cutting and feed forces against the cutting speed, the influence of the cutting speed on the chip thickness is smaller at higher cutting speeds of 950 and 1250 m/min, which demonstrates that the chip thickness is more affected by the cutting speed in CM than in HSM. On the other hand, as seen in Fig. 15, the variation of the chip thickness with the cutting edge radius is not significant especially under HSM conditions, and as a result, linear regression models fitting the chip thickness' results are not presented. Also, in CM, the magnitudes of the chip thickness are generally higher at larger edge radii.

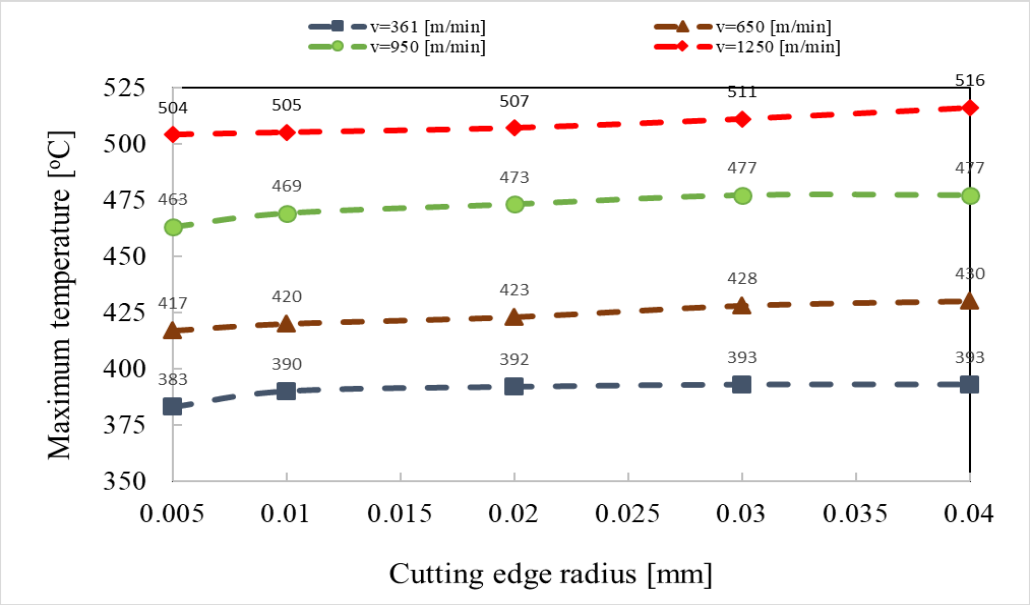

Fig. 12. The influence of cutting edge radius and cutting velocity on maximum cutting temperature.

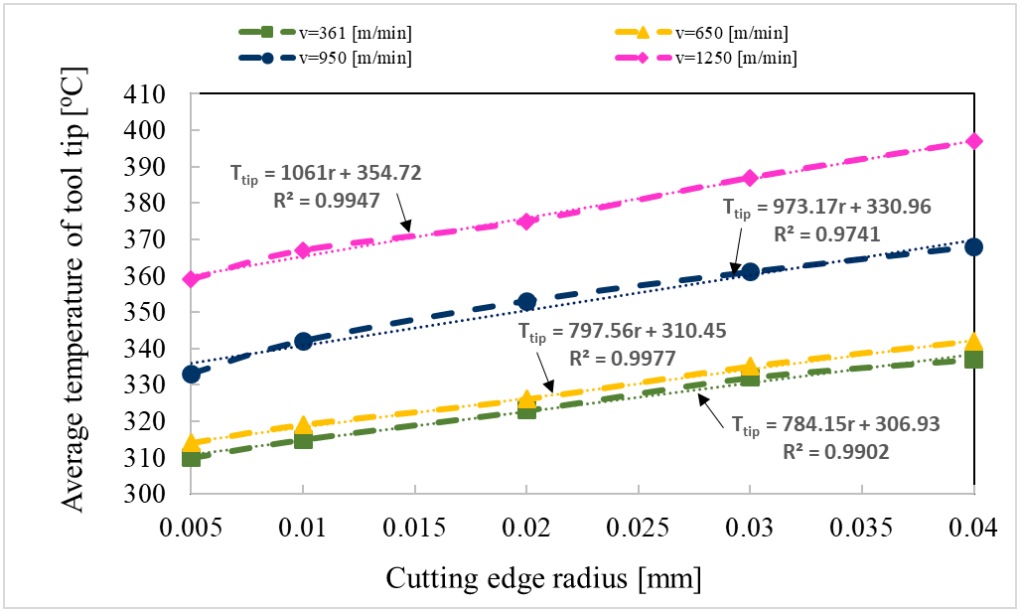

Fig. 13. The influence of cutting edge radius and cutting velocity on the average temperature of tool tip.

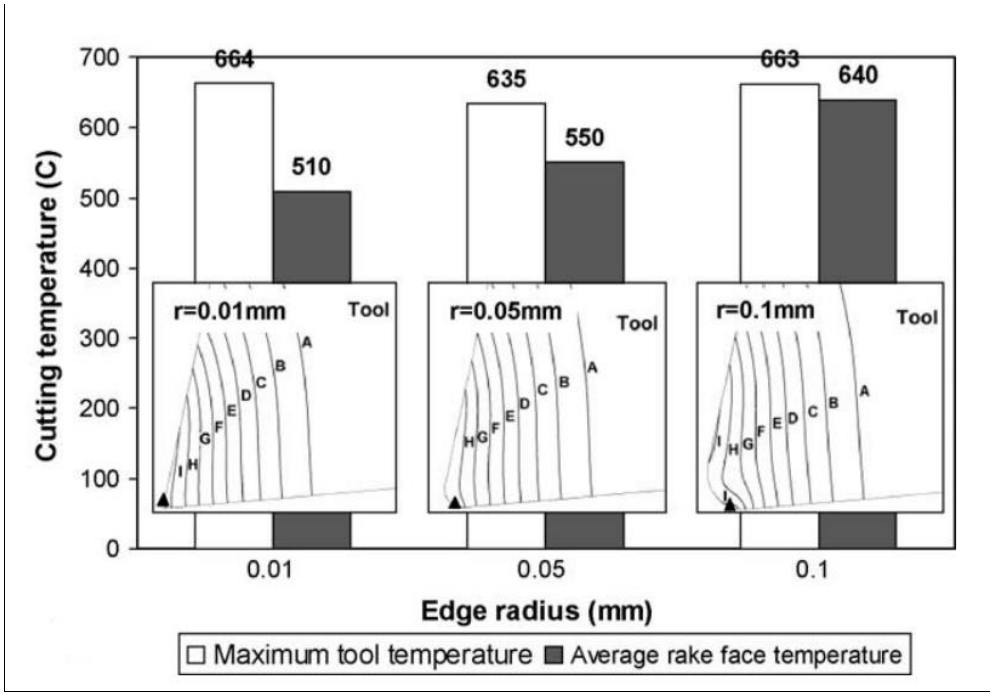
700
600
500
400
300
200
100
0
Cutting temperature (C)
664
510
635
550
663
640
r=0.01mm
Tool
r=0.05mm
Tool
r=0.1mm
Tool
A
B
C
D
E
F
G
H
I
0.01
0.05
0.1
Edge radius (mm)
Maximum tool temperature
Average rake face temperature

(a)

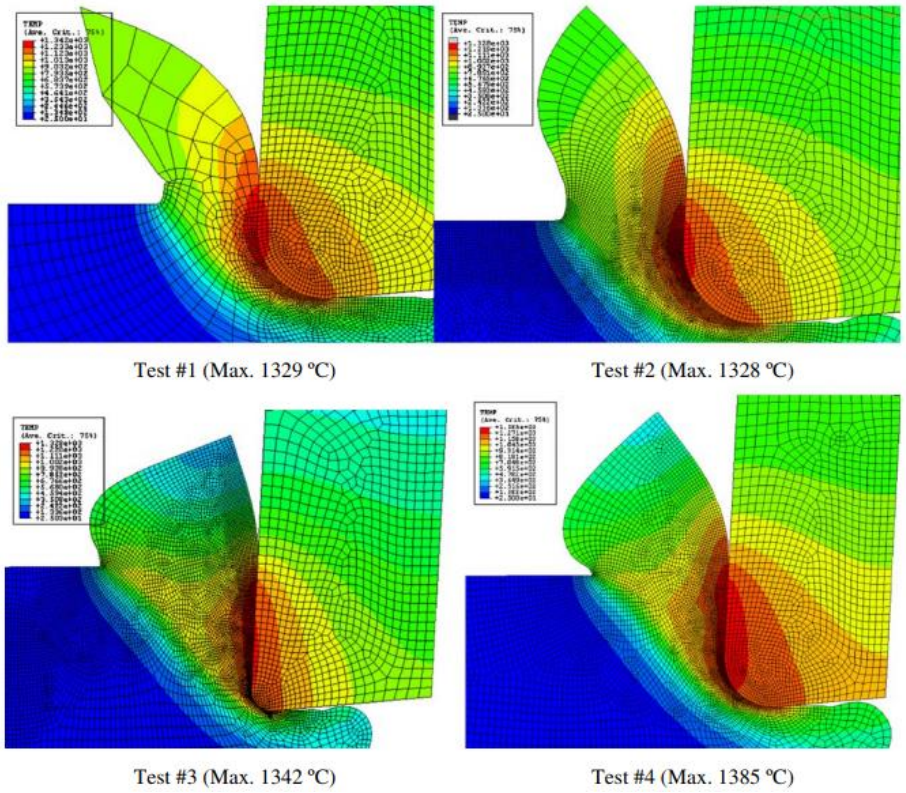
Test #1 (Max. 1329 ºC)
Test #2 (Max. 1328 ºC)
Test #3 (Max. 1342 ºC)
Test #4 (Max. 1385 ºC)

(b)

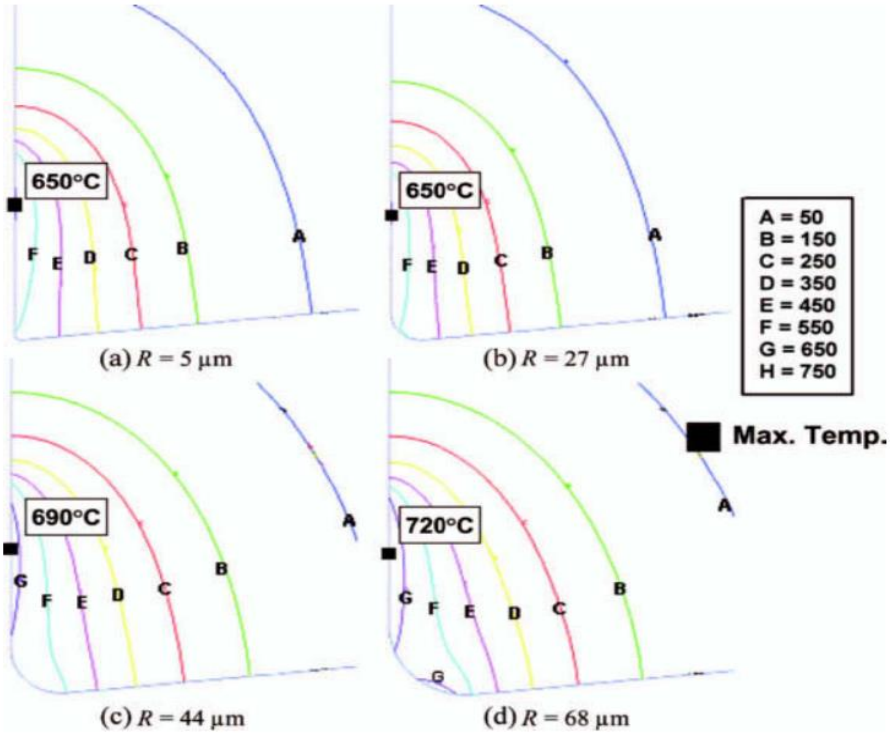

(c)

Fig. 14. The influence of the cutting edge radius on the cutting temperature in cutting of (a) AISI 1020 steel [1], (b) AISI 4340 steel [23], and (c) AISI 4142H steel [24].

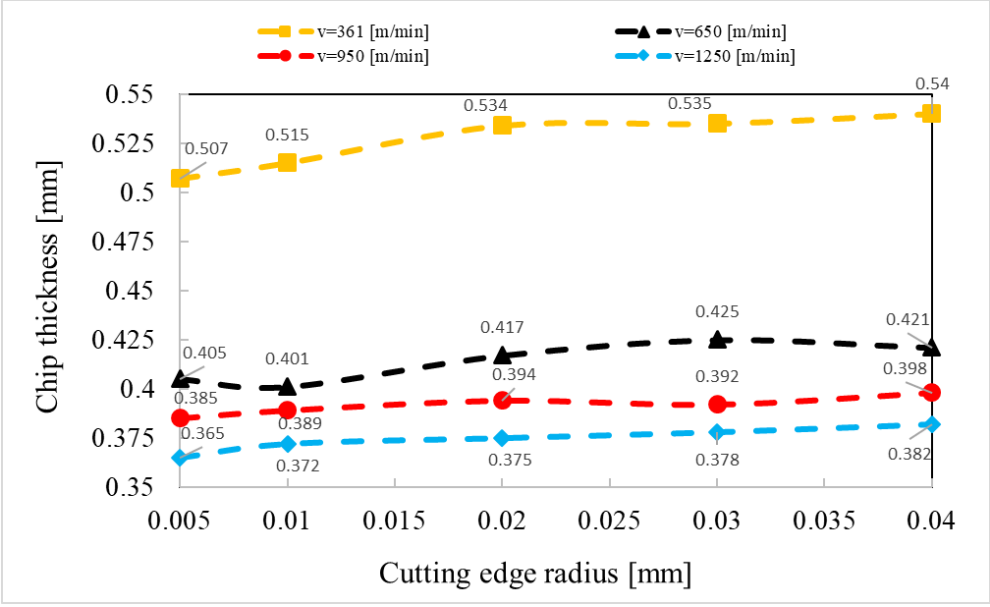

Fig. 15. The impact of cutting edge radius and cutting velocity on chip thickness.

5.2. Interaction between rake angle and cutting edge radius

The combined effects of rake angle and cutting edge radius on machining forces are shown in Figs. 16 and 17. It can be seen that the machining forces are strongly affected by the rake angle. The change in the rake angle from negative to positive values leads to reduced machining forces for all the cutting edge radii considered. This can be attributed to the reduction in the tool-chip contact pressure and friction when the rake angle changes from -8° to +8°. Also, as viewed in Figs. 16 and 17, with raising the cutting edge radius, machining forces increase for all the three rake angles.

More specifically, the slope of the linear model at the rake angle of -8° is larger for both cutting and feed forces (the slope is in turn 1421 and 2390 for cutting and feed forces), demonstrating that both cutting and feed forces are more sensitive to the cutting edge radius at a negative rake angle. Also, similar to the results obtained for the cutting speed, the percentage increase in the feed force is much larger than that in the cutting force for all the rake angles when the cutting edge radius is increased as the slopes of the linear models are much higher for the feed force compared with those for the cutting force.

The impacts of rake angle and cutting edge radius on cutting temperature are analyzed. As viewed in Figs. 18 and 19, both the maximum temperature occurring at the tool rake face and the average temperature of the tool tip decrease when the rake angle changes from negative to positive values for all the cutting edge radii under study. This reduction in the temperature can be attributed to the decrease in the tool-chip contact pressure and friction when the rake angle changes from -8° to +8°. Moreover, as seen in Figs. 18 and 19, for all the three rake angles under consideration, both the maximum temperature and the average temperature of the tool tip generally increase with increasing the cutting edge radius as also shown by the slopes of the linear models fitting the curves of the cutting temperature.

The effects of rake angle and cutting edge radius on chip thickness are illustrated in Fig. 20. The chip thickness decreases when the rake angle changes from negative to positive values for all the cutting edge radii under study. It is interesting to note that the variation of the chip thickness with the cutting edge radius is very small, concluding that the edge radius has a minor effect on the chip thickness.

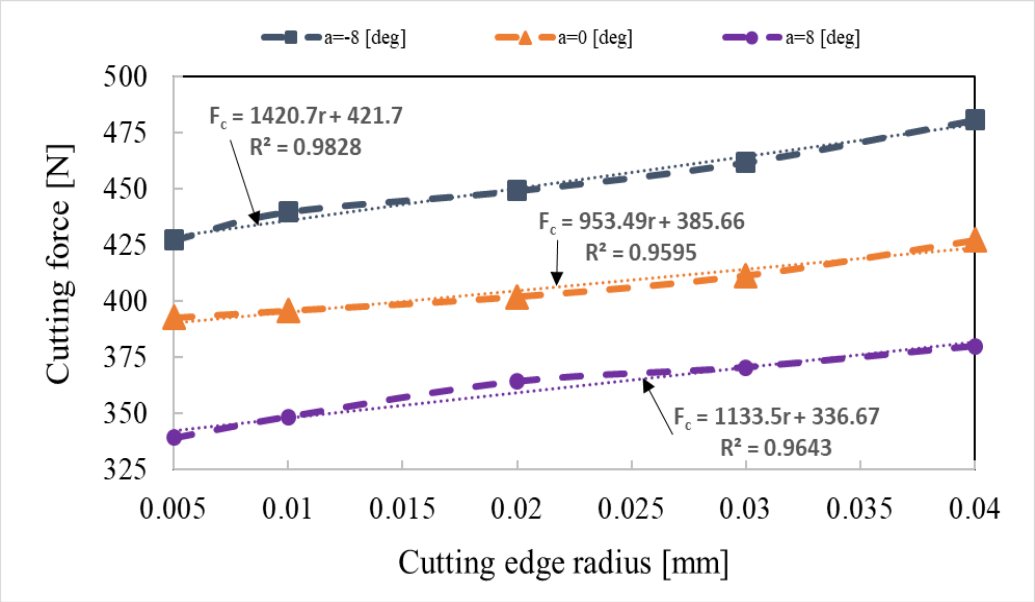

Fig. 16. The effect of cutting edge radius and rake angle on cutting force.

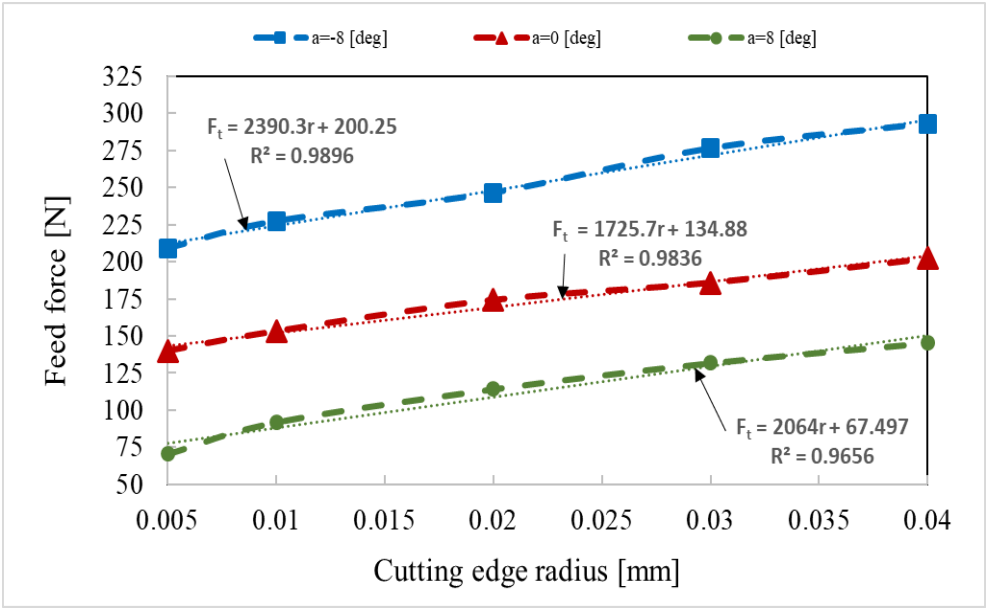

Fig. 17. The effect of cutting edge radius and rake angle on feed force.

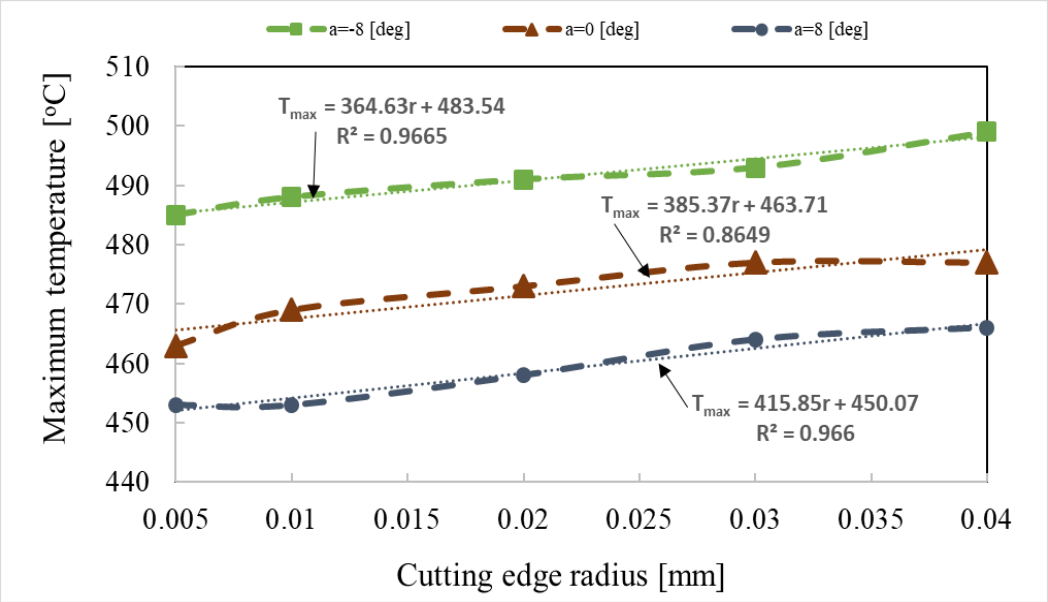

Fig. 18. The influence of cutting edge radius and rake angle on maximum temperature.

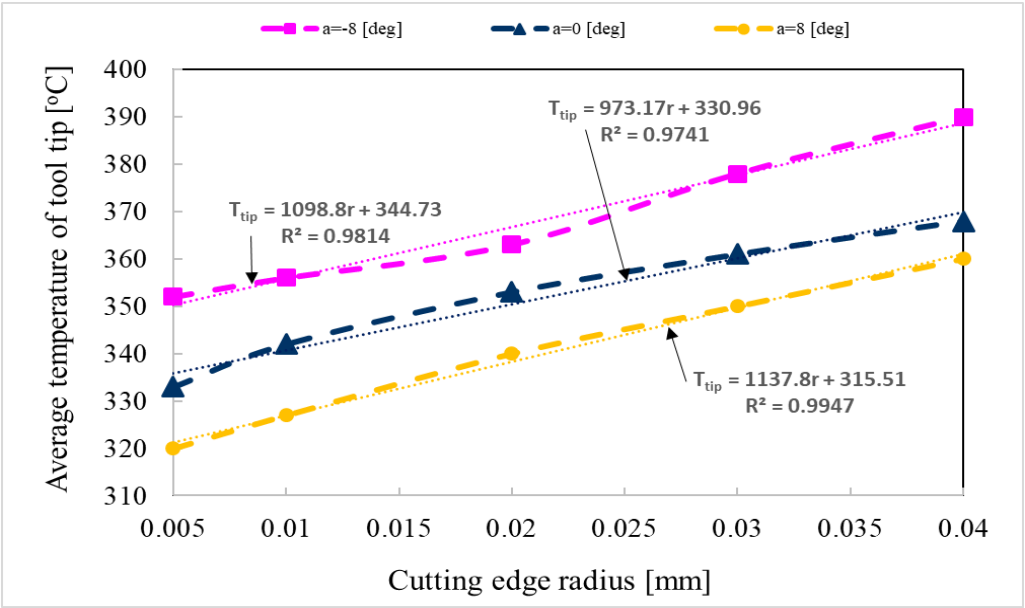

Fig. 19. The influence of cutting edge radius and rake angle on the average temperature of tool tip.

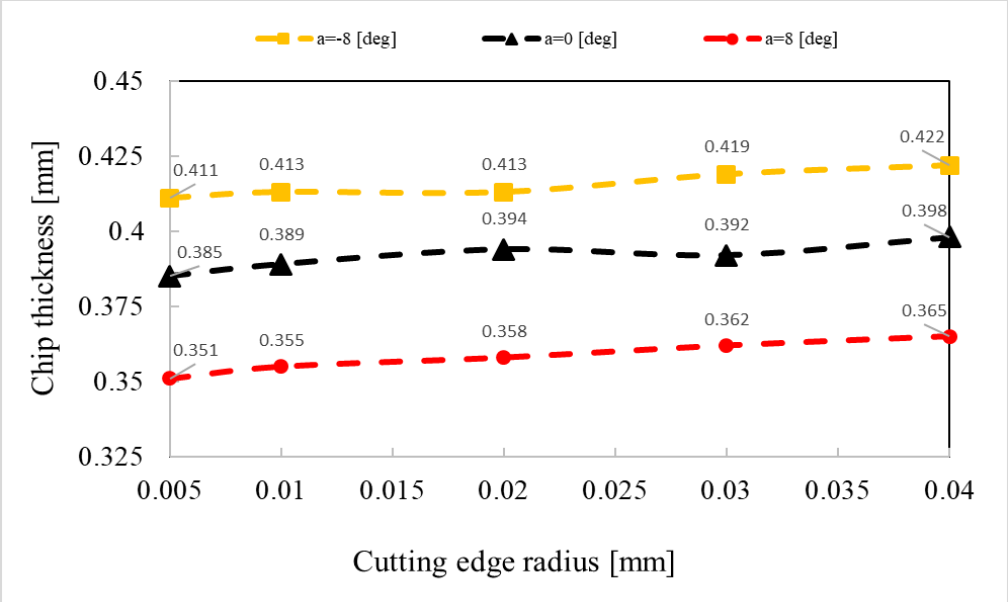

Fig. 20. The effect of cutting edge radius and rake angle on chip thickness.

5.3. Interaction between feed rate and cutting edge radius

Figures 21 and 22 show that at constant edge radius, the machining forces increase with raising the feed rate. These results are in agreement with those reported by Sadeghifar et al. [14], who reported that an increment in the feed rate increases the tool-chip contact area and directly raises the machining forces in cutting 300M steel. By contrast, a rise in the feed rate may indirectly reduce the cutting forces due to an increase in the frictional area, which produces more heat and softens the material [14]. In the cutting conditions considered herein, the contribution of the increase in the tool-chip contact area is larger than that of the increase in the frictional area, and as a result, the machining forces increase with the feed rate. Also, as seen in Figs. 21 and 22, with raising the cutting edge radius, the machining forces increase for all the feed rates under study. More particularly, similar to the results obtained for the analysis of the cutting speed and rake angle, the percentage increase in the feed force is much larger than that in the cutting force for all the feed rates when the cutting edge radius is increased. This shows that the influence of the cutting edge radius on the feed force is larger than that on the cutting force.

The effects of feed rate and cutting edge radius on the maximum temperature and the average temperature of the tool tip are shown in Figs. 23 and 24, where it can be seen that both temperatures increase with the feed rate. It is known that an increment in the feed rate increases the tool-chip contact area, and as a result, increases the frictional heat, which raises the machining temperature. Furthermore, for all the feed rates under study, the average temperature of the tool tip increases with increasing the cutting edge radius. The maximum temperature also generally increases with the edge radius. However,

the percentage increase in the average temperature of the tool tip is much higher than that in the maximum temperature when the cutting edge radius increases.

The chip thickness increases with raising the feed rate as displayed in Fig. 25. Increasing the feed rate increases the cutting area, and consequently, increases the chip thickness. Also, similar to the results for the cutting speed and rake angle, the variation of the chip thickness with the cutting edge radius is very small.

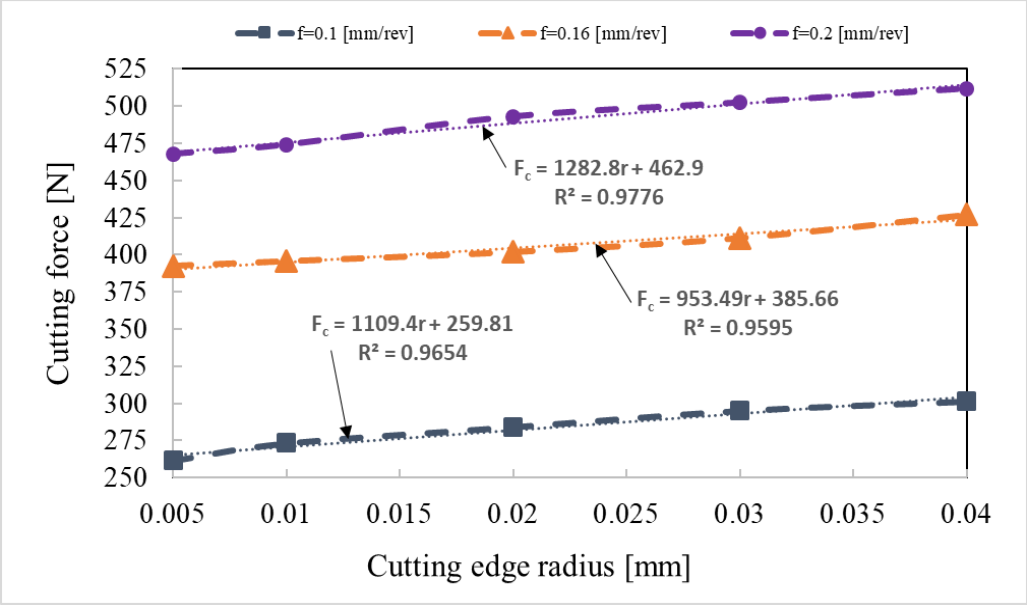

Fig. 21. The influence of cutting edge radius and feed rate on cutting force.

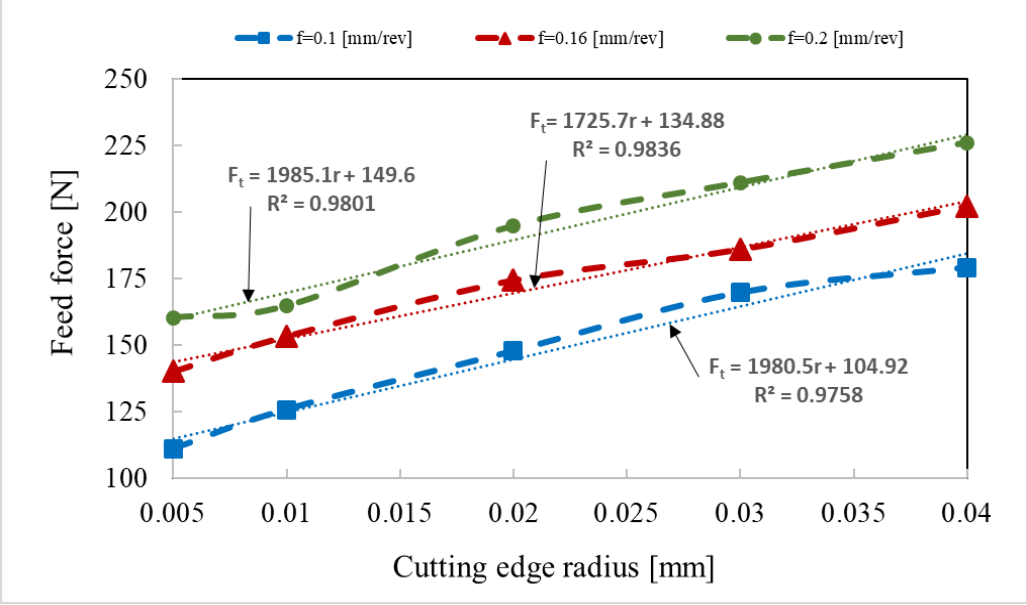

Fig. 22. The influence of cutting edge radius and feed rate on feed force.

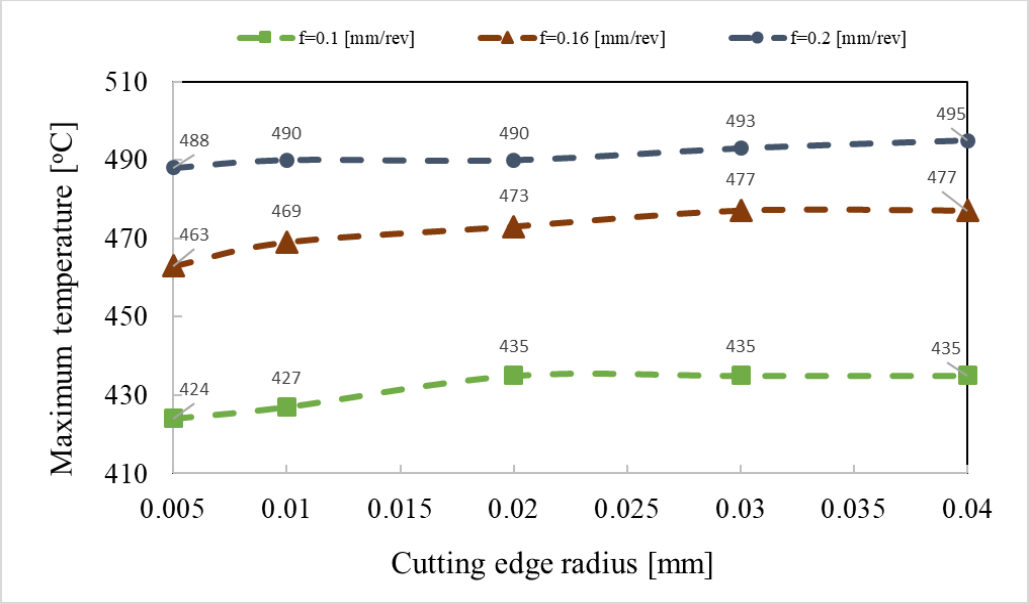

Fig. 23. The impact of cutting edge radius and feed rate on maximum temperature.

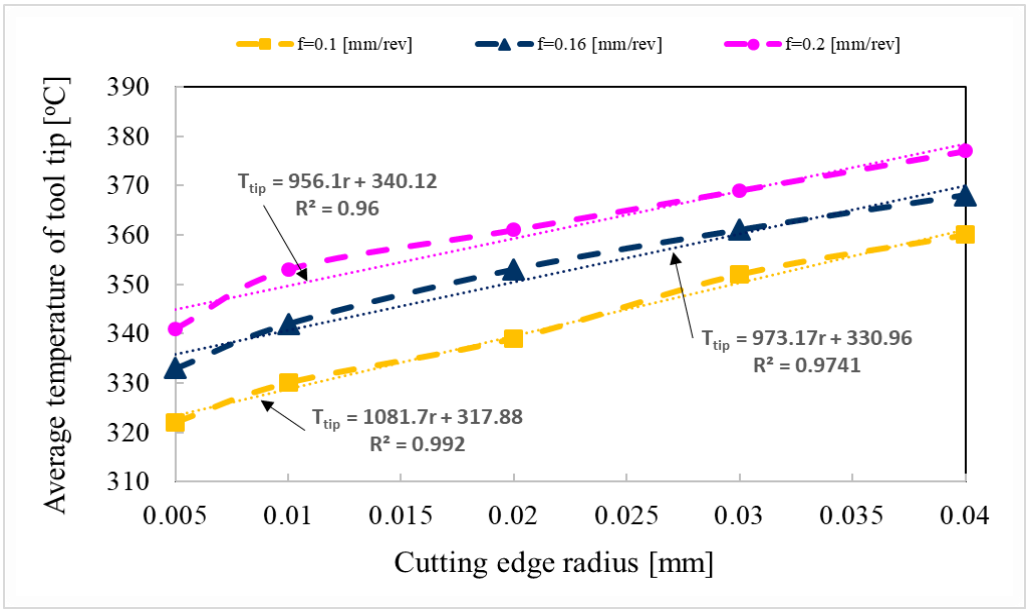

Fig. 24. The impact of cutting edge radius and feed rate on the average temperature of tool tip.

6. Summary and conclusions

In this research study, the impact of tool's cutting edge radius on machining forces, cutting temperature, and chip thickness was investigated in orthogonal straight turning of aluminum alloys 6061-T6 for various cutting speeds, rake angles and feed rates using FEM. The FE simulations were performed using the DEFORM® software. Special attention was given to study the effect of the cutting edge radius

on machining characteristics and comparison of the results in CM and HSM. The FE model was validated with the experimental tests for several machining conditions. The results demonstrated that both cutting and feed forces were more sensitive to the cutting edge radius at low cutting speeds (related to CM) and also at a negative rake angle. It was also found that the location of the maximum cutting temperature and the sensitivity of the maximum cutting temperature to the cutting edge radius in cutting of metals depend more on cutting conditions and tool geometry than workpiece and tool materials. Also, the maximum cutting temperatures remained nearly constant with increasing the tool edge radius, whereas the average temperatures of the tool tip clearly increased particularly in HSM. Finally, the results obtained for various cutting speeds, rake angles, and feed rates showed that the variation of the chip thickness with the cutting edge radius was slight, especially in HSM. These results provide the industry with some insight into the design of tool geometry to improve the machining charactrestics including machining forces, cutting tempetarure and chip morphology. Accurate predictions of machining forces and temperature are crucial for selecting the optimal machining parameters to improve the machining efficiency and the surface integrity of components as the end goal of the machining industry. Moreover, the developed finite element model can be utilized as a predictive reliable tool for industrial applications to avoid conducting too many expensive, time-consuming experimental tests, which will be more desirable and economical to the industrial environments.

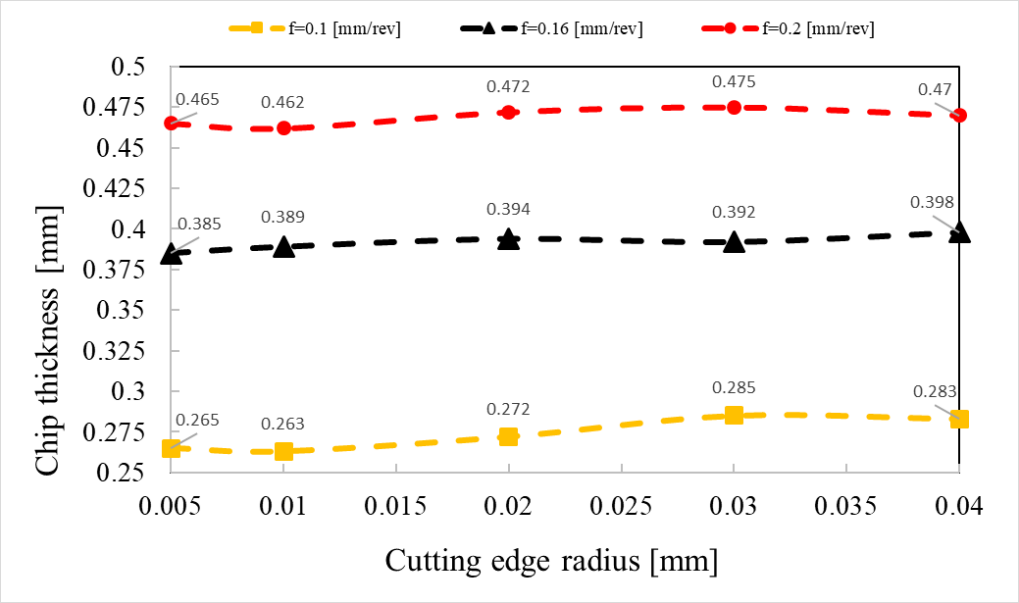

Fig. 25. The influence of cutting edge radius and feed rate on chip thickness.

Acknowledgments

The authors would like to thank the Aluminium Research Centre (REGAL) for financial support of part of the present research work.

References

[1] Yen YC, Jain A, Altan T (2004) A finite element analysis of orthogonal machining using different tool edge geometries. J Mater Process Technol 146:72-81.

[2] Özel T. Experimental and finite element investigations on the influence of tool edge radius in machining nickel-based alloy. ASME 2009 International Manufacturing Science and Engineering Conference, West Lafayette, Indiana, USA, 2009.

[3] Wyen CF, Wegener K (2010) Influence of cutting edge radius on cutting forces in machining titanium. CIRP annals 59:93-96.

[4] Daoud M, Chatelain JF, Bouzid A (2015) Effect of rake angle on Johnson-Cook material constants and their impact on cutting process parameters of Al2024-T3 alloy machining simulation. Int J Adv Manuf Technol 81:1987-1997.

[5] Cheng X, Xuming Z, and Jiang F (2016) Optimizing the geometric parameters of cutting edge for rough machining Fe-Cr-Ni stainless steel. Int J Adv Manuf Technol 85:683-693.

[6] Akram S, Imran H, Khan M, Mubashar A, Warsi S, Riaz U. A numerical investigation and experimental validation on chip morphology of Aluminum Alloy 6061 during orthogonal machining. 2016 Moratuwa Engineering Research Conference (MERCon), IEEE, Moratuwa, Sri Lanka, 2016.

[7] Zhuang K, Weng J, Zhu D, Ding H (2018) Analytical modeling and experimental validation of cutting forces considering edge effects and size effects with round chamfered ceramic tools. J Manuf Sci Eng 140:081012-1 (16 pages).

[8] Reddy MM, Kumar BM, Kumaraesan S (2018) Finite element analysis and modeling of temperature distribution in turning of titanium alloys. Metal Mater Eng 24:59-69.

[9] Emamian A. The effect of tool edge radius on cutting conditions based on updated Lagrangian formulation in finite element method. MS thesis, McMaster University, 2018.

[10] Patel JP. Finite element studies of orthogonal machining of aluminum alloy AA2024-T351. MS thesis, The University of North Carolina, Charlotte, 2018.

[11] Mir A, Luo X, Cheng K, Cox A (2018) Investigation of influence of tool rake angle in single point diamond turning of silicon. Int J Adv Manuf Technol 94:2343-2355.

[12] Jiang L, Wang D (2019) Finite-element-analysis of the effect of different wiper tool edge geometries during the hard turning of AISI 4340 steel. Simul Model Pract Theory 94:250-263.

[13] Sadeghifar M, Sedaghati R, Jomaa W, Songmene V (2018) A comprehensive review of finite element modeling of orthogonal machining process: Chip formation and surface integrity predictions. Int J Adv Manuf Technol 96:3747-3791.

[14] Sadeghifar M, Sedaghati R, Jomaa W, Songmene V (2018) Finite element analysis and response surface method for robust multi-performance optimization of radial turning of hard 300M steel. Int J Adv Manuf Technol 94:2457-2474.

[15] Miguélez MH, Soldani X, Molinari A (2013) Analysis of adiabatic shear banding in orthogonal cutting of Ti alloy. Int J Mech Sci *75*:212-222.

[16] Chen Y, Li H, Wang J (2015) Analytical modelling of cutting forces in near-orthogonal cutting of titanium alloy Ti6Al4V. Proc Inst Mech Eng, Part C: J Mech Eng Sci 229:1122-1133.

[17] Daoud M, Jomaa W, Chatelain JF, Bouzid A, Songmene V (2014) Identification of material constitutive law constants using machining tests: a response surface methodology based approach. WIT Trans Built Env 137:25-36.

[18] Roy P, Sarangi SK, Ghosh A, Chattopadhyay AK (2009) Machinability study of pure aluminium and Al-12% Si alloys against uncoated and coated carbide inserts. Int J Ref Metal Hard Mater 27:535-544.

[19] Daoud M, Jomaa W, Chatelain JF, Bouzid A (2015) A machining-based methodology to identify material constitutive law for finite element simulation. Int J Adv Manuf Technol 77:2019-2033.

[20] Filice L, Micari F, Rizzuti S, Umbrello D (2007) A critical analysis on the friction modelling in orthogonal machining. Int J Mach Tools Manuf 47:709-714.

[21] Ucun I, Aslantas K (2011) Numerical simulation of orthogonal machining process using multilayer and single-layer coated tools. Int J Adv Manuf Technol 54:899-910.

[22] Pawade RS, Joshi SS, Brahmankar PK (2008) Effect of machining parameters and cutting edge geometry on surface integrity of high speed turned Inconel 718. Int J Mach Tools Manuf 48:15-28.

[23] Özel T, Zeren E (2007) Finite element modeling the influence of edge roundness on the stress and temperature fields induced by high-speed machining. Int J Adv Manuf Technol 35:255-267.

[24] Al-Zkeri I, Rech J, Altan T, Hamdi H, Valiorgue F (2009) Optimization of the cutting edge geometry of coated carbide tools in dry turning of steels using a finite element analysis. Mach Sci Technol 13:36-51.